

## ARTICLE

# Dual-branch dense network for seismic background noise elimination

**Wei Wang<sup>1</sup> , Haoliang Chen<sup>2</sup>, Dekuan Chang<sup>1</sup>, Xinyang Wang<sup>3\*</sup> ,  
Shujiang Wang<sup>1</sup>, and Dong Li<sup>1</sup>**

<sup>1</sup>Geophysics Institute, Research Institute of Petroleum Exploration and Development-Northwest, PetroChina, Lanzhou, Gansu, China

<sup>2</sup>Northeast Electric Power Design Institute CO., LTD. of China Power Engineering Consulting Group, Changchun, Jilin, China

<sup>3</sup>Department of Communication Engineering, College of Electric Engineering, Northeast Electric Power University, Jilin City, Jilin, China

(This article belongs to the *Special Issue: Advanced Artificial Intelligence Theories and Methods for Seismic Exploration*)

## Abstract

Distributed acoustic sensing (DAS) has attracted much attention in seismic data acquisition because of its low cost, anti-electromagnetic interference, and high acquisition density. Unfortunately, the acquired DAS records are usually accompanied by various kinds of complex noise, affecting subsequent interpretation and inversion. Traditional methods have difficulties in effectively attenuating the intense background noise. In general, the denoising task of DAS data is challenging. Recently, convolutional neural networks (CNNs) exhibit a good ability in suppressing the noise in DAS records. However, traditional CNN-based frameworks always have a relatively simple network architecture, bringing negative impacts on the denoising capability. To solve this problem, we propose a dual-branch dense network (DBD-Net) in this paper. Specifically, DBD-Net introduces a novel combination of dual-branch modules and an attention mechanism: the dual-branch modules extract multi-scale coarse-to-fine features, while the attention mechanism highlights the most informative features. This joint design strengthens feature representation and signal recovery compared with conventional CNN structures such as denoising CNN (DnCNN) and U-Net. Moreover, an attention module is employed to enhance the effective features. To verify the denoising ability, we compare DBD-Net with other competing methods, including band-pass filter, DnCNN, and U-Net, in terms of denoising capability and processing accuracy. Experimental results verify that DBD-Net can improve the quality of DAS records with a signal-to-noise ratio increment of nearly 26 dB. Meanwhile, the intense DAS background noise is also perfectly suppressed and the weak signals are effectively restored, representing advantages over the competing methods.

**Keywords:** Background noise suppression; Distributed acoustic sensing; Convolutional neural network; Vertical seismic profile; Signal-to-noise ratio improvement

### \*Corresponding author:

Xinyang Wang  
(wxy23@neepu.edu.cn)

**Citation:** Wang W, Chen H, Chang D, Wang X, Wang S, Li D. Dual-branch dense network for seismic background noise elimination. *J Seismic Explor.* 2025;34(5):53-65.  
doi: 10.36922/JSE025290038

**Received:** July 20, 2025

**1st revised:** September 18, 2025

**2nd revised:** October 23, 2025

**Accepted:** October 24, 2025

**Published online:** November 24, 2025

**Copyright:** © 2025 Author(s). This is an Open-Access article distributed under the terms of the Creative Commons Attribution License, permitting distribution, and reproduction in any medium, provided the original work is properly cited.

**Publisher's Note:** AccScience Publishing remains neutral with regard to jurisdictional claims in published maps and institutional affiliations.

## 1. Introduction

Distributed acoustic sensing (DAS), by capturing the phase change of Rayleigh scattered light in optical fibers, is capable of accurately detecting subtle ground deformations induced by artificial seismic waves. Compared with traditional geophones, it exhibits advantages in acquisition properties and has been extensively used for seismic exploration, mainly combined with the vertical seismic profiles technique.<sup>1-3</sup> Unfortunately, effective signals acquired by the DAS system are relatively weak and are often susceptible to interference from strong background noise.<sup>4</sup> In addition, the DAS noise has complicated characteristics, and a few of them are not observed in the seismic records acquired by the geophones, such as fading noise, horizontal noise, and coupling noise.<sup>5-8</sup> It means that the traditional denoising methods might be unable to accurately attenuate this specific noise, leading to a degradation in denoising performance.<sup>9,10</sup> Therefore, effectively suppressing seismic noise and recovering effective signals has become a key aspect of seismic data processing.

Recently, researchers proposed many denoising methods to process seismic data, and some remarkable results have been achieved. In general, traditional denoising methods are classified into four categories: time-frequency analysis methods,<sup>11,12</sup> signal-decomposition-based methods,<sup>13</sup> multi-scale analysis methods,<sup>14,15</sup> and low-rank-based methods.<sup>16,17</sup> First, the time-frequency analysis methods can detect the effective signals by utilizing the differences in physical or spectral properties between signal and noise components. Typical methods include the band-pass filter (BPF),<sup>18</sup> median filter,<sup>19</sup> and Wiener filter.<sup>20</sup> Their denoising principles are relatively idealized. Thus, their performance might degrade when processing intense DAS background noise. Aiming to enhance the denoising ability, signal-decomposition-based methods, such as empirical mode decomposition,<sup>21</sup> variational mode decomposition,<sup>22,23</sup> and singular value decomposition,<sup>24</sup> were proposed. Generally speaking, these methods can decompose the signal into different modes and then accomplish the denoising task by retaining the signal-dominant modes. However, the signals and noise have overlaps, which limit the decomposition accuracy. Therefore, extracting the signal components from the mixed mode is often difficult and significantly affects the denoising performance. Meanwhile, multi-scale analysis methods are another type of commonly used denoising approach in the exploration industry. The application of these methods considers the fact that seismic signals and background noise have distinct characteristics in sparsity. In other words, we can use multi-scale analysis, such as shearlet,<sup>14,25,26</sup> seislet,<sup>27</sup> and curvelet transform,<sup>28</sup> to convert the temporal signals into

a given sparse domain, and apply a 2D filter to maintain the signal components. Unfortunately, it is difficult to determine the critical parameters. Inappropriate thresholds or filters will inevitably cause signal leakage or residual noise. Furthermore, the low-rank-based approach is based on the assumption that the matrices of pure signals have low-rank properties. Rank is increased by the presence of DAS noise.<sup>16,17</sup> Therefore, the denoising task is equivalent to an optimization problem, which aims to obtain the minimal rank and output the attenuation results. Although low-rank-based methods can provide great denoising performance, the determination of optimal rank and huge computational cost still hinder the wide application of these methods. In summary, traditional denoising methods all have their shortcomings, and the attenuation accuracy cannot be ensured when faced with low signal-to-noise ratio (SNR) DAS data.

Nowadays, deep-learning-based methods are widely used in the field of seismic data processing.<sup>29-32</sup> Some successful applications have been reported in waveform inversion,<sup>33,34</sup> classification,<sup>35,36</sup> interpolation,<sup>37</sup> and migration.<sup>38-40</sup> As one of the hot topics in deep learning, the convolutional neural network (CNN) has been applied to DAS background noise attenuation. Dong *et al.*<sup>9</sup> proposed a method based on denoising CNNs (DnCNNs) to suppress the noise of seismic data, which optimizes the parameters and training data of DnCNNs so that they can adapt to the desert seismic data denoising environment and achieve adaptive blind denoising. The feasibility of CNNs in seismic data denoising was also verified through experiments.<sup>41</sup> Liu *et al.*<sup>42</sup> applied U-Net in seismic data noise suppression to achieve more effective seismic data processing through multi-scale extraction and channel expansion. Moreover, they verified the effectiveness of U-Net in seismic signal recovery and intense noise attenuation. These studies demonstrate the effectiveness of CNN in seismic data processing and show the superiority over traditional denoising methods at the same time. Its excellent performance is mainly benefited from the network structure and training data. The shortage of high-quality training data is certainly an important potential problem for CNN-based methods. It is well recognized that acquiring pure signals from field data is infeasible, posing a significant challenge in constructing signal training dataset. In addition, low-quality training data always impacts the signal amplitude preservation and weak signal recovery. Although carefully designed datasets can mitigate this issue, the fundamental limitation still lies in the network's ability to effectively extract and utilize the features of DAS data. This highlights the need for more advanced architectures.

To enhance the processing accuracy, a novel dual-branch dense network (DBD-Net) is proposed. Unlike previous CNN-based frameworks with relatively simple architectures that limit denoising capability, our method employs dual-branch modules to extract both coarse and fine features at multiple scales. In addition, a dense module is introduced to alleviate the gradient disappearance and improve feature fusion, while an attention mechanism is designed to enhance effective signals under complex noise conditions. With these improvements, the proposed network cannot only suppress intense DAS background noise but also preserve weak seismic signals more effectively. Therefore, compared with conventional CNN models such as DnCNN and U-Net, our method provides a more targeted solution for DAS denoising. The paper consists of four parts. Section 1 is the introduction, which introduces the significance of the study and the current status of the study. Section 2 is the method, which introduces the CNN network designed in this paper and the process of constructing a high-quality training set. Section 3 presents the results, which demonstrate the effectiveness of DBD-Net through the comparison experiments of synthetic and field records. Section 4 is the conclusion of this paper.

## 2. Methods

Figure 1 shows DBD-Net's network structure. In general, DBD-Net consists of the dual-branch module, the dense module, and the attention module. Specifically, DBD-Net has two network branches, a main scale, and a self-attention module. In the main scale, five convolutional layers are first applied to capture the initial features. Then,

the dual-branch module, shown in Figure 2, is used to capture the multi-scale features. Meanwhile, the dense module transfers the shallow features, aiming to fuse them with deep features and improve the feature representation. In addition, a self-attention module is used to assist the effective feature extraction. Next, we will detail the specific descriptions of the network components.

### 2.1. DB module

Figure 2 presents the structure of the dual-branch module. The dual-branch module has double branches, designed to achieve multi-scale feature extraction. Specifically, the top branch focuses on capturing local fine features, while the bottom branch captures global coarse features. In the top branch, the feature map is first up-sampled by bilinear interpolation. Then, the dilated convolutional layers with different dilation rates (*i.e.*, 2, 3, 5), alternated with regular convolutional layers, are used to capture detailed local features in DAS data. Meanwhile, skip connections are used to transfer and fuse the features. Here, the application of dilated convolution rapidly enlarges the receptive field, and the utilization of different dilation rates maintains the diversity of captured features and avoids feature loss caused by the chessboard effect. In the bottom branch, the feature map is first down-sampled using max-pooling, which reduces its resolution to highlight coarse structures. Then, the same set of dilated convolutional layers, alternated with regular convolutional layers, is applied to capture global features. Skip connections are also employed to transfer and fuse features at this scale. Finally, the outputs of the top and bottom branches are added with the initial input of

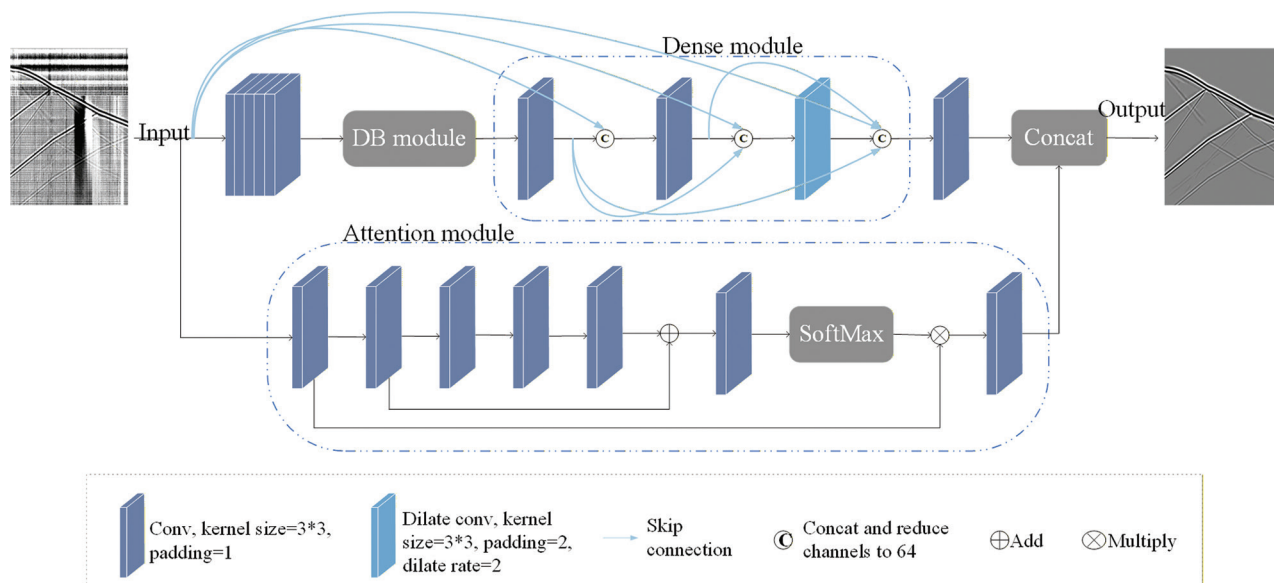


Figure 1. Structure of DBD-Net

Abbreviations: DB Module: Dual-branch module; DBD-Net: Dual-branch dense network.

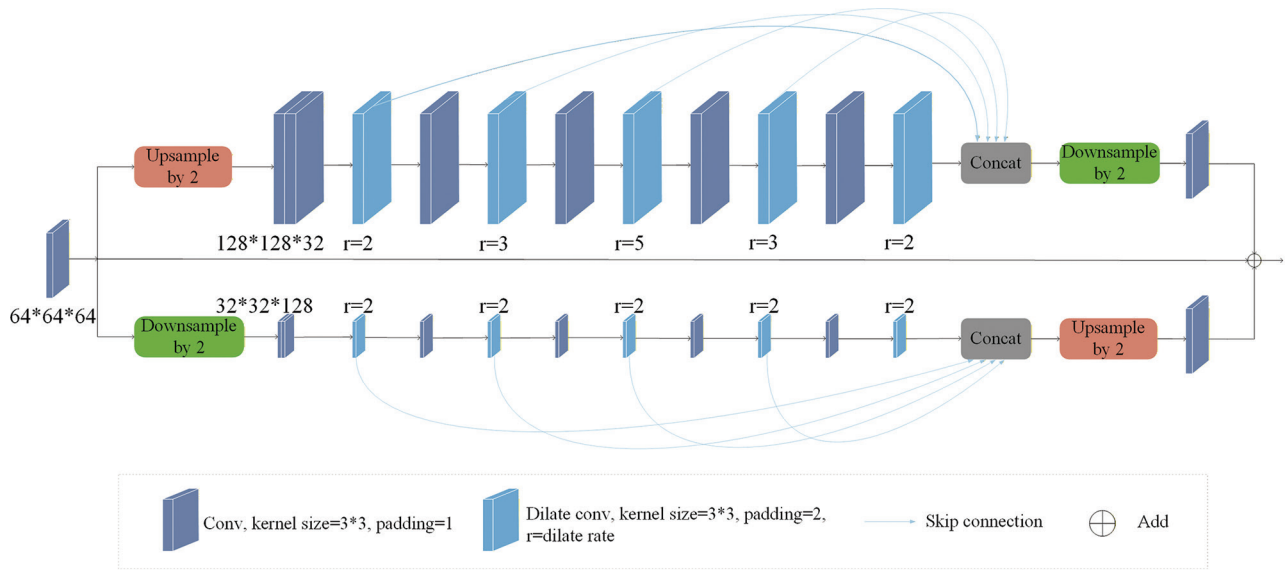


Figure 2. Structure of dual-branch module

the dual-branch module to enhance the effective features and reduce data redundancy.

## 2.2. Dense module

In general, with the depth of the network increasing, the learnable features are inundated with redundant information, which undoubtedly results in gradient disappearance and local optimum problems. The shallow features can reduce data redundancy and have good maintenance for gradients. In this study, we design a dense module, as depicted in Figure 1, to transfer and merge shallow features with deep features. The dense module has three convolutional layers, and all the outputs of convolutional layers are concatenated with the initial input data of the network through skip connections. It means that the feature utilization ability is enhanced and the gradient disappearance phenomenon is relieved, thereby improving the effective features.

## 2.3. Attention module

Effective signals in DAS data are commonly heavily affected by complex noise. To enhance the feature extraction capability, we design a spatial attention module. Specifically, the features are extracted using six convolutional layers, and then shallow feature fusion is implemented using skip connections. A softmax function is then used to activate the output of the sixth convolutional layer and distributions of the captured features. On this basis, the distributions are used as the weights to multiply with input features, and then, the desired features are enhanced because the effective features always have a larger probability value.

Finally, the output of the attention module works as the guidance information to concatenate with the output of the main scale, thereby highlighting the primary features and improving the denoising accuracy, particularly for the weak up-going signals. In summary, the function of the attention module is to suppress noise-related features and emphasize effective seismic signals, significantly enhancing the recovery of weak events in complex DAS records.

## 2.4. Seismic denoising principle

In this study, we used DBD-Net to denoise noisy DAS records, and the detailed principle is shown below. The expression of the noisy DAS record is shown as follows:

$$y = x + n \quad (I)$$

where  $y$  denotes the noisy data,  $x$  and  $n$  represent the effective signals and background noise, respectively. Subsequently,  $y$  is used as the network input. The network output is an estimation of the effective signal, which is expressed as follows:

$$\hat{x} = F(y; \zeta) \quad (II)$$

where  $\hat{x}$  denotes the estimation of the effective signal,  $F$  is the high-dimensional nonlinear mapping relationship constructed by the DBD-Net, with network parameters of  $\zeta = \{\omega, k\}$ . Here,  $\omega$  is the weight, and  $k$  denotes bias. The network parameters are obtained randomly at the beginning, and the estimation error of the effective signal is quite large at this time. Then, we need to construct a loss function to evaluate error, which is defined as follows:



$$L_2(\zeta) = \frac{1}{N} \sum_{i=1}^N \|F(y_i; \zeta) - x_i\|^2 \quad (\text{III})$$

Where  $y_i$  is the noisy record and  $x_i$  is the effective signal. We can iteratively optimize the parameters by using the backpropagation strategy. After training the network for several epochs, the error converges and becomes stable. In this study, we selected a set of parameters that minimize the loss function as the optimal set of parameters  $\zeta_{out}$ . The final denoising results are given as follows:

$$\hat{x}_{out} \approx x = F(y; \zeta_{out}) \quad (\text{IV})$$

## 2.5. Construction of the training set

Our training dataset contains a clean set of pure signal data and a set of field noise data. The pure signal dataset is simulated by simple seismic wavelets as in other previous studies, which have some differences from the properties of field DAS signals. It means that the performance of the trained models cannot be guaranteed and even recover some fake events in some conditions. To improve the denoising performance, we generated the clean signal training dataset using the forward modeling method. Specifically, it uses seismic wavelets to excite the artificial velocity model. Meanwhile, we utilized the finite difference method to simulate the propagation of the wavefield and then obtained synthetic data. To ensure the accuracy of learnable features, the previously acquired seismic profiles were considered references in the construction of velocity models. In this study, there were 20 velocity models. We obtained a total of 160 clean synthetic records. Table 1 presents the modeling parameters. The modeling equations of the Ricker Wavelet are described as:

$$L(t) = A \cdot \left[ 1 - 2\pi \cdot f(t - t_0)^2 \right] \cdot e^{-[\pi \cdot f_0(t - t_0)]^2} \quad (\text{V})$$

where  $A$  is the amplitude,  $t_0$  and  $f_0$  denote the initial time and dominant frequency, respectively. As shown in Figure 3, we provide an example of a velocity model and synthetic recording. The inverted triangle at the top right identifies the source location, while the black line on the

left symbolizes the receiving line, as shown in the figure. Subsequently, the synthetic records were divided into  $64 \times 64$  patches. The signal dataset consisted of 20000 patches. For the field noise dataset, the passive source data acquired in Northeast China were employed. Similarly, the field noise data were divided into noise patches by the  $64 \times 64$  sliding window. Here, we selected 30000 patches randomly to generate the test dataset. The field noise patches were multiplied by a weight ranging from 1 to 8 and then added with signal patches to form the noisy patches in the training process. We input signal patches and noise patches into DBD-Net, and through this training process, we successfully obtained denoising models. Figure 4 shows some samples of pure signal and field noise patches.

## 2.6. Training details

In general, the high-performance computation technique affects CNN-based methods' performance. In this work, a graphics workstation was built with a configuration consisting of Intel (R) Core (TM) i5-9400F, NVIDIA GeForce RTX 2060 Super, and 16GB RAM. The specific parameters are listed in Table 2.

## 3. Results

### 3.1. Synthetic data results

Figure 5 shows the results concerning the synthetic DAS record, with Figure 5A presenting the corresponding velocity model, which has four layers, for the synthetic DAS record shown in Figure 5B. The fundamental frequency of the Ricker wavelet is 40 Hz.

Figure 5C shows the field seismic noise, which was combined with the synthetic DAS record to yield the noisy record, as shown in Figure 5D, which was used as the analyzed data. Here, we used BPF, DnCNN,<sup>43</sup> and U-Net,<sup>44</sup> for experimental comparison to process the noisy data with the proposed DBD-Net. Specifically, the pass band of BPF is 20–90 Hz, while DnCNN and U-Net use the same strategy and dataset as DBD-Net to train the denoising models.

The noisy data is shown in Figure 6A. BPF (Figure 6B) cannot effectively suppress the complex DAS noise, whose limited performance is demonstrated by the signal leakage and residual horizontal noise. Compared with BPF, CNN-based frameworks always provide better denoising results and the weak signals can also be restored. Among these methods, DnCNN and U-Net (Figure 6C and D) are outperformed by DBD-Net (Figure 6E). Notably, recovered events in DBD-Net are continuous and smooth, indicating its advantages in intensive DAS noise suppression. On this basis, two areas of interest are enlarged, as shown in Figure 7, for detailed comparisons. Area 1 is the local

**Table 1. Forward modeling parameters**

| Parameters                  | Value          |
|-----------------------------|----------------|
| Seismic wavelet             | Ricker wavelet |
| Seismic wave frequency (Hz) | 20–110         |
| Wave velocity (m/s)         | 800–4700       |
| Trace space (m)             | 1              |
| Offset (m)                  | 100–300        |
| Sampling interval (s)       | 0.0004         |

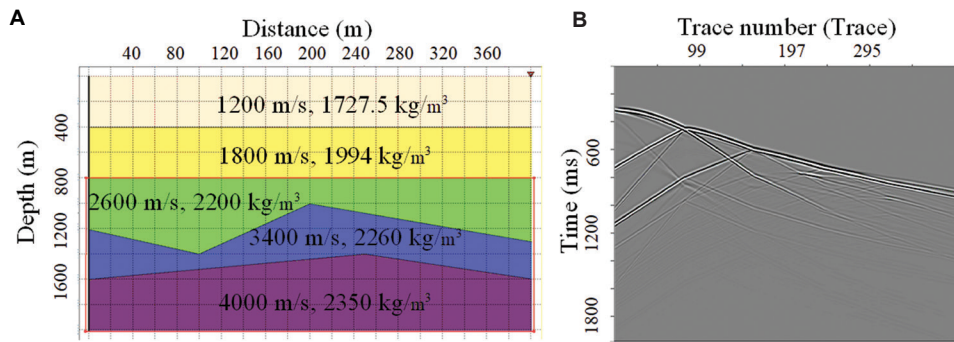


Figure 3. Clean synthetic record. (A) Forward model. (B) Synthetic record.

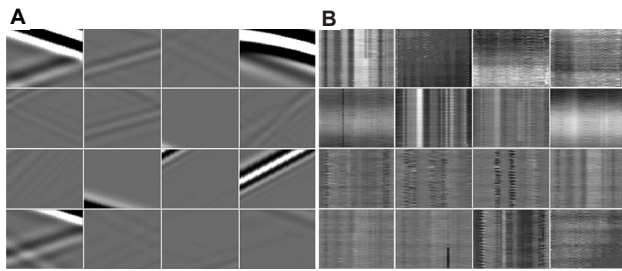


Figure 4. Samples of the training dataset. (A) Clean and noisy signal patches. (B) Noisy signal patches.

Table 2. Network architecture parameters

| Hyper-parameter         | DnCNN                         | U-Net                         | DBD-Net                       |
|-------------------------|-------------------------------|-------------------------------|-------------------------------|
| Optimizer               | ADAM                          | ADAM                          | ADAM                          |
| Patch size              | 64×64                         | 64×64                         | 64×64                         |
| Batch size              | 32                            | 32                            | 32                            |
| Epoch                   | 60                            | 60                            | 60                            |
| Learning rate range     | $[10^{-4}, 10^{-5}, 10^{-6}]$ | $[10^{-4}, 10^{-5}, 10^{-6}]$ | $[10^{-4}, 10^{-5}, 10^{-6}]$ |
| Input channels          | 1                             | 1                             | 1                             |
| Layers                  | 17                            | 19                            | 22                            |
| Convolution kernel size | $3 \times 3 \times 64$        | $3 \times 3 \times 64$        | $3 \times 3 \times 64$        |

Abbreviations: DBD-Net: Dual-branch dense network;  
DnCNN: Denoising convolutional neural network.

record (900–1200 traces) ranging from 1.5 to 1.8 s, which is contaminated by complex optical noise, while area 2 is the local record (240–540 traces) between 1.3 and 1.7 s, which is dominated by weak reflection events (Figure 7A). Similar results could be observed that BPF is affected by disordered information (Figure 7B), which also brings difficulty for the recognition of weak signals. Although DnCNN can effectively attenuate the background noise to some extent, the recovered events are corrupted and few weak signals have been recovered (Figure 7C). In addition, U-Net (Figure 7D) and DBD-Net represent close denoising ability; however, the recovered signals of DBD-Net are more complete and smoother (Figure 7E), indicating the

impressive performance of DBD-Net in intensive DAS noise suppression.

Meanwhile, the F-K spectral analysis was conducted to compare the denoising method from the spectral perspective. As shown in Figure 8A, there is a conspicuous aliasing phenomenon between the clean signals and field noise. BPF (Figure 8B) shows limited effects when confronted with aliasing noise, and only noise components out of the pass band could be attenuated. The comparisons for the CNN-based frameworks can be achieved from two aspects: signal recovery performance and noise attention ability. On the one hand, there are obvious signal leakage components in the filtered noise results of DnCNN and U-Net (Figure 8C and 8D), demonstrating the adverse effect on signal amplitude preservation during the denoising process. On the other hand, the reconstructed results of DBD-Net (Figure 8E) have the most similar properties as the clean signals, indicating its capability in intensive DAS noise suppression. In summary, the comparisons in the F-K domain illuminate the superiority of DBD-Net.

In addition, a quantitative analysis was performed to further investigate the performance of each denoising method. In signal processing, SNR and root-mean-square-error (RMSE) are two key metrics for evaluating the denoising effect, and their specific expressions are as follows:

$$SNR = 10 \lg \left( \frac{\sum_{i=1}^n \sum_{j=1}^m S_{ij}^2}{\sum_{i=1}^n \sum_{j=1}^m (N_{ij} - S_{ij})^2} \right) \quad (VI)$$

$$RMSE = \sqrt{\frac{1}{mn} \sum_{i=1}^n \sum_{j=1}^m (N_{ij} - S_{ij})^2} \quad (VII)$$

where  $S$  represents the clean record, and  $N$  represents the denoising result. In addition,  $i$  and  $j$  represent the

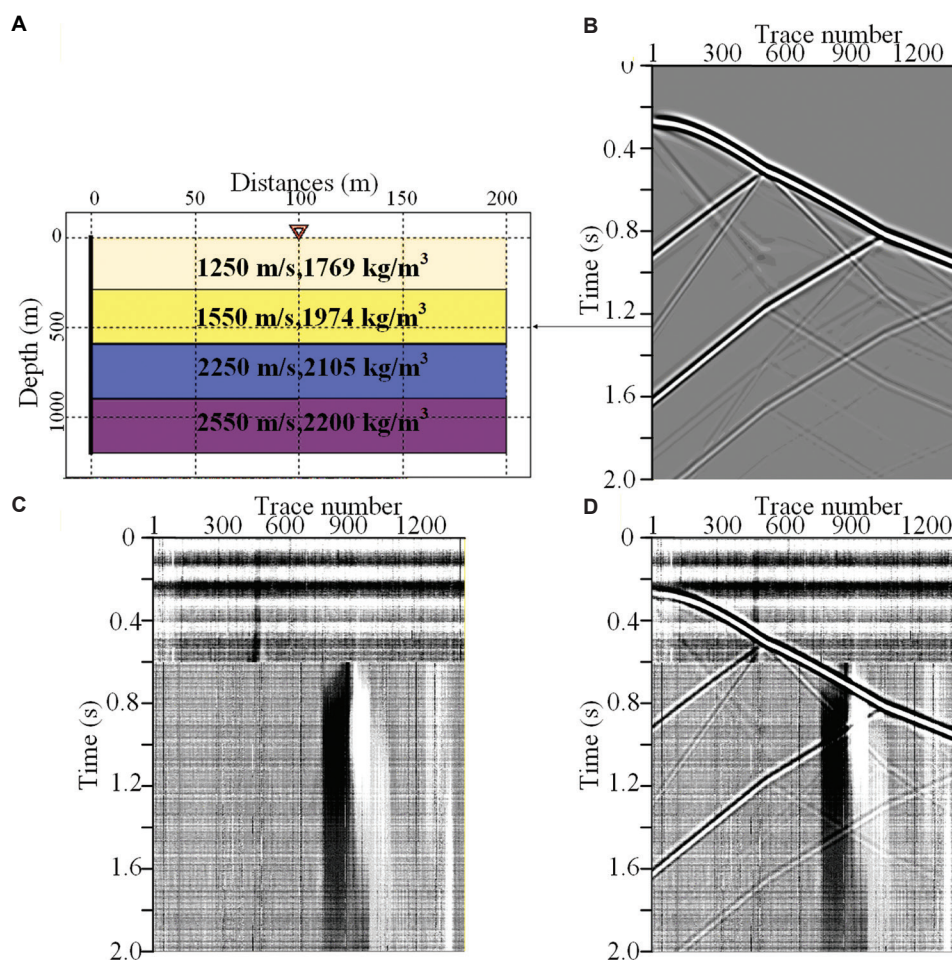


**Figure 5.** The synthetic DAS record for the test. (A) Forward model. (B) Synthetic clean seismic record. (C) Added noise. (D) Noisy DAS record with an SNR of 0 dB.

Abbreviations: DAS: Distributed acoustic sensing; SNR: Signal-to-noise ratio.

dimensions of the synthetic record. From the expressions, it can be seen that SNR is more inclined to measure the denoising effect, and a higher SNR means that the method is more capable of denoising. Meanwhile, RMSE is able to evaluate the effective signal maintenance ability, and a lower RMSE implies that the corresponding method is good at preserving the effective signal. To further investigate the denoising performance, we processed synthetic recordings with different SNRs. Table 3 presents the SNR and RMSE results for different methods. BPF has the lowest SNR increment among all the denoising methods, indicating its limited noise suppression ability. In contrast, the CNN-based methods have better performance, demonstrating significant SNR increment and small RMSE value. Under the same training environment, the training time of DnCNN, U-Net, and our proposed DBD-Net is about 1.26 h, 0.73 h, and 0.94 h, respectively. Although DBD-Net

takes slightly longer to train than U-Net, the SNR improves by almost 3 dB. Compared with other methods, DBD-Net can increase the SNR by nearly 26 dB, reflecting its superiority in noise attenuation. Similar trends are also observed in RMSE results, indicating the effectiveness of DBD-Net in signal amplitude preservation.

### 3.2. Field data results

Figure 9 shows the results of the noise suppression. To better demonstrate the performance of DBD-Net in practical applications, the field DAS records in Figure 9A were processed using DBD-Net and other aforementioned methods. Specifically, the field DAS record, acquired in Northeast China, contains 1360 traces of seismic data. The corresponding sampling frequency is 2500 Hz. The reflection events in this field DAS record are severely corrupted by complex DAS interference, such as fading



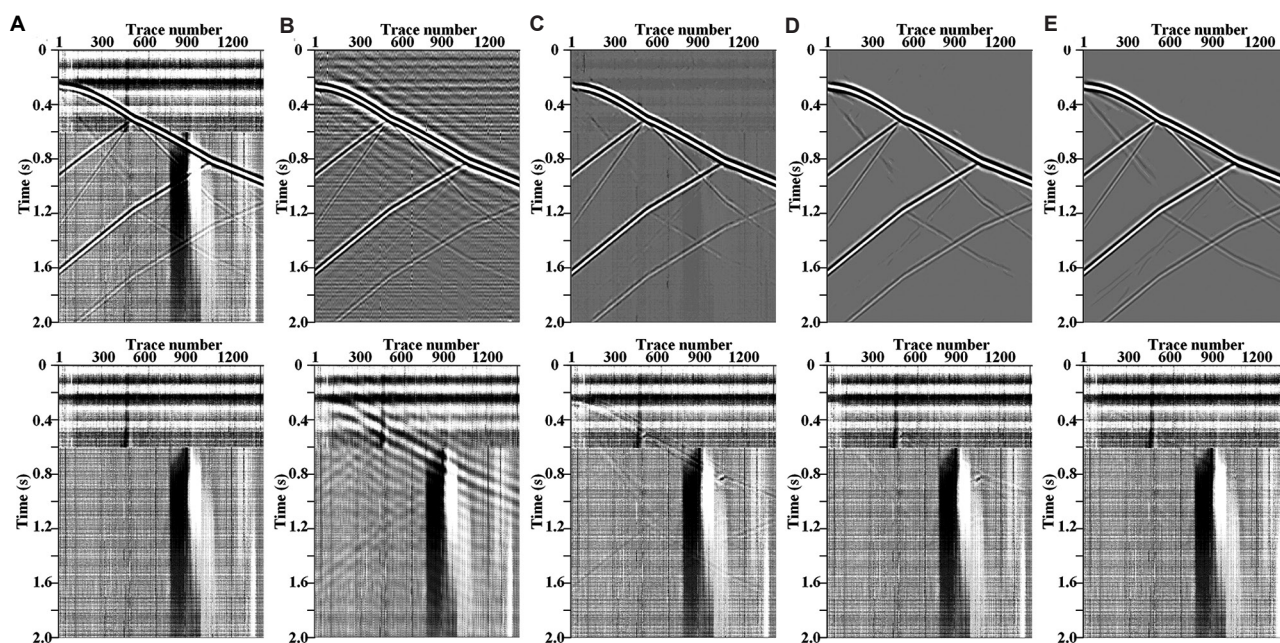


**Figure 6.** Synthetic record processing results. (A) Noisy record with an SNR of 0 dB and field data. (B) Results of BPF (10.24 dB). (C) Results of DnCNN (18.43 dB). (D) Results of U-Net (23.24 dB). (E) Results of DBD-Net (26.09 dB).

Abbreviations: BPF: Band-pass filter; DBD-Net: Dual-branch dense network; DnCNN: Denoising convolutional neural network; SNR: Signal-to-noise ratio.

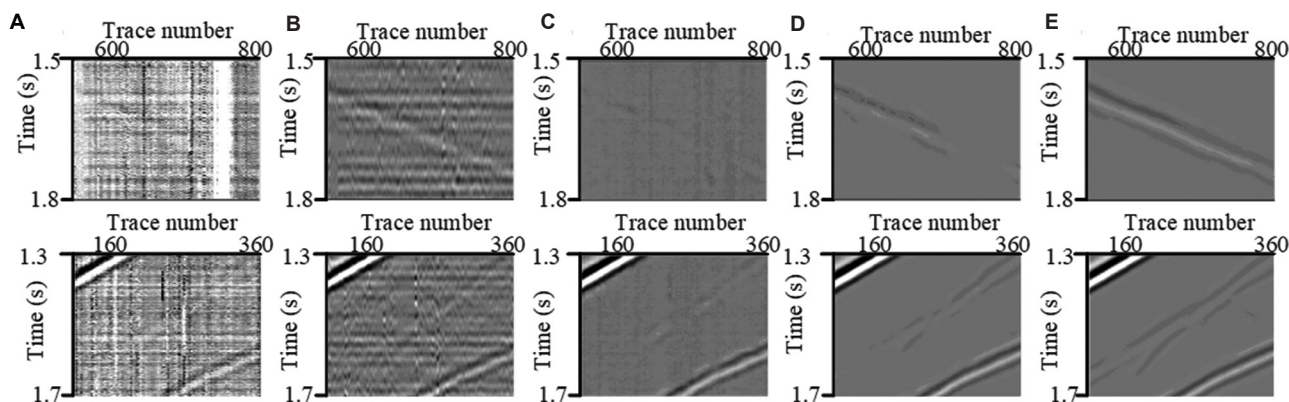


**Figure 7.** Enlarged figures showing denoising results corresponding to Figure 6. (A) Noisy record (top: Area 1, bottom: Area 2). (B–E) Results of BPF (B), DnCNN (C), U-Net (D), and DBD-Net (E) (top: Area 1, bottom: Area 2).

Abbreviations: BPF: Band-pass filter; DBD-Net: Dual-branch dense network; DnCNN: Denoising convolutional neural network.

noise and time-varying optical noise. It is known that BPF, as depicted in Figure 9B, cannot suppress the background noise in the pass band, resulting in residual horizontal noise and disordered recovered events. Moreover, as shown in Figure 9C, DnCNN has limited performance in DAS noise elimination, and the residual noise still influences the recognition of reflection signals, especially for weak up-going events. Although U-Net outperforms DnCNN (Figure 9D), the remained fading noise still

affects the denoising results. In contrast, DBD-Net has a clear background with continuously recovered events (Figure 9E), indicating its great performance in denoising complex DAS data.

To further evaluate the denoising performance, we enlarged a local record (1000–1360 traces), ranging from 0.93 to 1.33 s as shown in Figure 10A. Similar to the results in Figure 9, BPF is incapable of suppressing the DAS background noise (Figure 10B). Meanwhile, as shown in



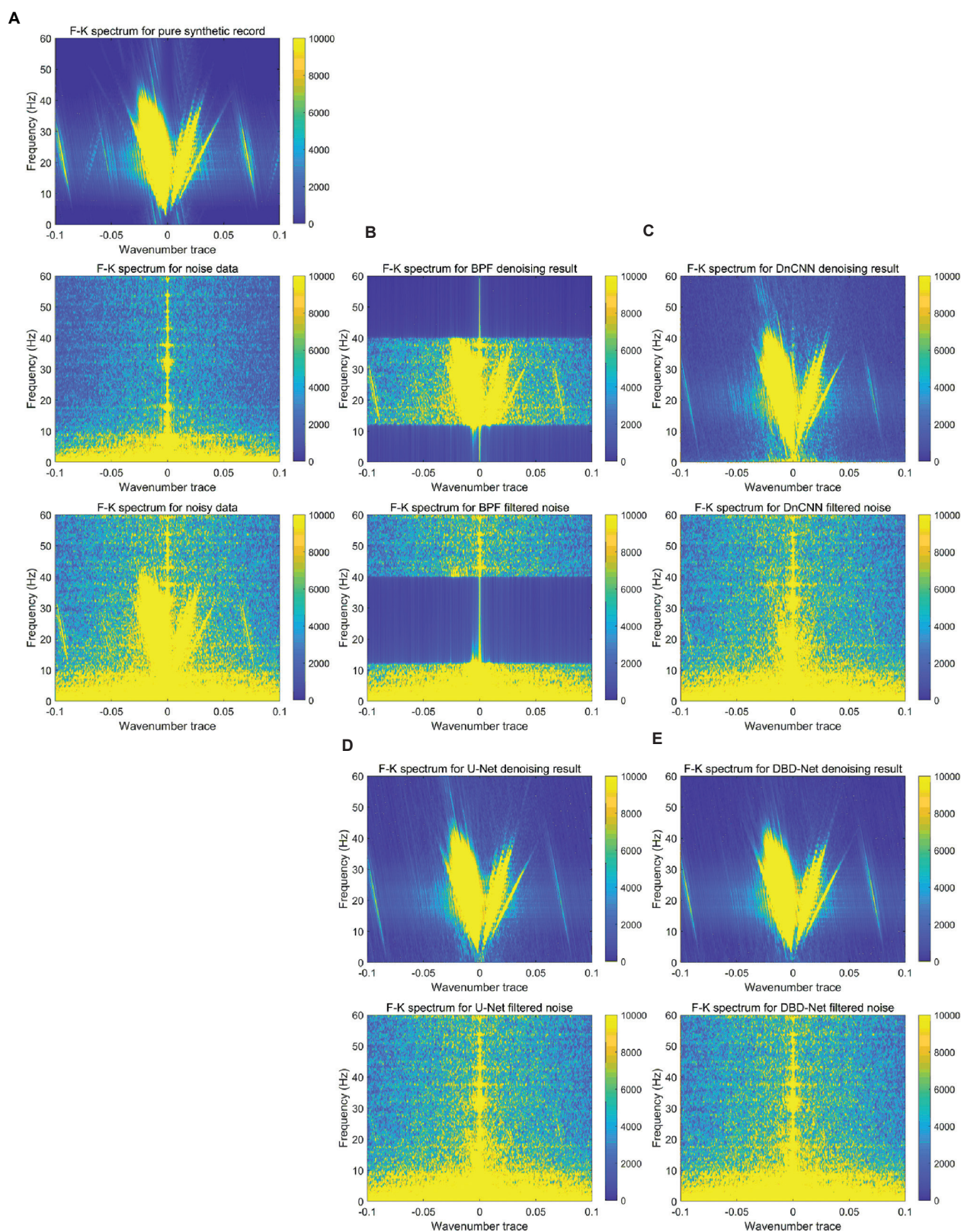


**Figure 8.** F-K spectral analysis. (A) F-K spectra of the clean record, noise data, and noisy data. (B–E) F-K spectra for the denoising results and filtered noise obtained by BPF (B), DnCNN (C), U-Net (D), and DBD-Net (E).

Abbreviations: BPF: Band-pass filter; DBD-Net: Dual-branch dense network; DnCNN: Denoising convolutional neural network.

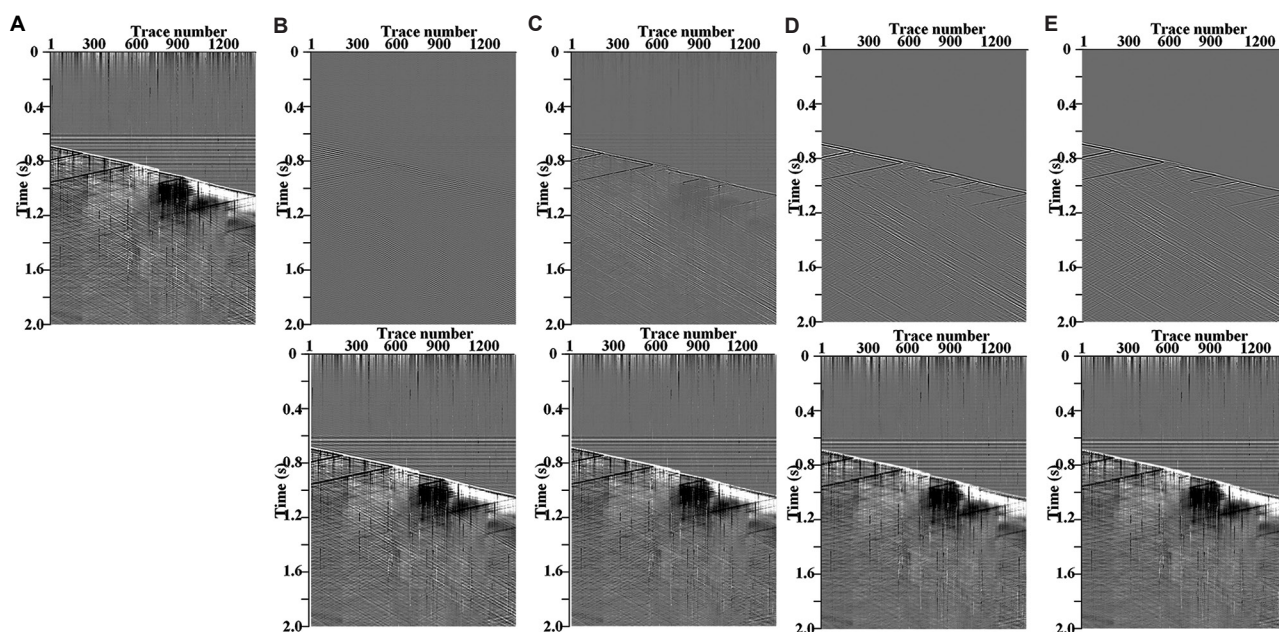


**Figure 9.** Field DAS records results. (A) Field DAS records. (b) Results of BPF. (C) Results of DnCNN. (D) Results of U-Net. (E) Results of DBD-Net. Abbreviations: BPF: Band-pass filter; DAS: Distributed acoustic sensing; DBD-Net: Dual-branch dense network; DnCNN: Denoising convolutional neural network.

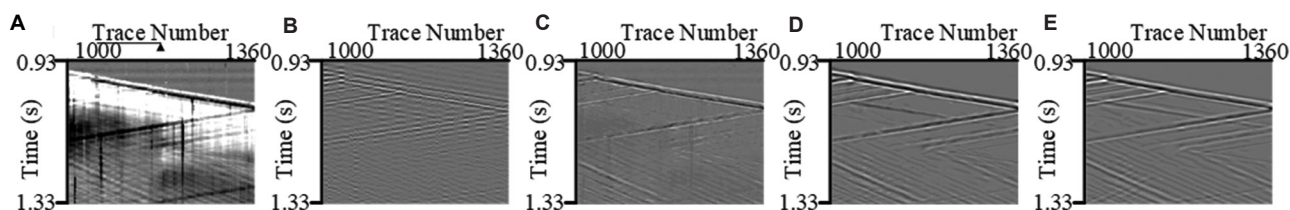


**Figure 10.** Enlargements of denoising results in Figure 9. (A) Field DAS records. (B) Results of BPF. (C) Results of DnCNN. (D) Results of U-Net. (E) Results of DBD-Net.

Abbreviations: BPF: Band-pass filter; DAS: Distributed acoustic sensing; DBD-Net: Dual-branch dense network; DnCNN: Denoising convolutional neural network.

**Table 3. Comparison of SNR and RMSE among different algorithms**

| Synthetic record (dB) | BPF      |        | DnCNN    |        | U-Net    |        | DBD-Net  |        |
|-----------------------|----------|--------|----------|--------|----------|--------|----------|--------|
|                       | SNR (dB) | RMSE   | SNR (dB) | RMSE   | SNR (dB) | RMSE   | SNR (dB) | RMSE   |
| 0                     | 10.24    | 0.2674 | 18.43    | 0.1041 | 23.24    | 0.0599 | 26.09    | 0.0431 |
| -2                    | 9.08     | 0.3056 | 17.27    | 0.1191 | 22.55    | 0.0648 | 25.46    | 0.0464 |
| -4                    | 7.71     | 0.3578 | 15.99    | 0.1378 | 21.70    | 0.0714 | 24.71    | 0.0505 |
| -6                    | 6.16     | 0.4277 | 14.58    | 0.1623 | 20.71    | 0.0807 | 23.81    | 0.0561 |
| -8                    | 4.47     | 0.5196 | 12.88    | 0.1973 | 19.60    | 0.0910 | 22.69    | 0.0638 |
| -10                   | 2.68     | 0.6387 | 10.94    | 0.2466 | 18.32    | 0.1055 | 21.36    | 0.0744 |

Abbreviations: BPF: Band-pass filter; DBD-Net: Dual-branch dense network; DnCNN: Denoising convolutional neural network; RMSE: Root-mean-square-error; SNR: Signal-to-noise ratio.

Figure 10C, DnCNN also performs below expectations, producing corrupted and discontinuous recovered signals. Among these methods, U-Net and DBD-Net, as displayed in Figure 10D and E, demonstrate similar denoising performance. However, DBD-Net is more competent

in intense DAS noise elimination because of the clear background and smooth reconstructed events. Therefore, this analysis has proven the effectiveness of DBD-Net in denoising the complex DAS records, not only in noise attenuation but also in signal recovery.



## 4. Discussion

In this paper, we propose a CNN-based method named DBD-Net for seismic data denoising. Unlike traditional methods such as BPF, DBD-Net is capable of capturing complex seismic features and attenuating intense noise. Compared with representative CNN architectures such as DnCNN and U-Net, the main novelty of DBD-Net lies in the introduction of dual-branch modules for multi-scale feature extraction, together with a dense module for feature fusion and an attention mechanism for emphasizing effective signals. This design enables the network to more effectively restore weak seismic events while suppressing strong background noise.

Moreover, the noise dataset used in this study was collected from field DAS records and contains multiple types of interference, such as horizontal noise and fading noise. The experimental results show that DBD-Net maintains stable performance across these noise conditions, verifying its practical applicability. From a computational perspective, although training is relatively time-consuming due to the multi-branch design, the inference stage is efficient and suitable for practical denoising. In the future, lightweight strategies such as model pruning will be investigated to further reduce computational overhead and enhance deployment feasibility under different acquisition conditions.

## 5. Conclusion

In this study, we propose a novel multiscale denoising network that incorporates a multiscale scheme and an attention mechanism. Specifically, the proposed network uses a dual-branch module to extract coarse and detailed features in seismic data from multi-scale inputs. The attention module highlights and extends the primary features, thus improving the denoising ability. Meanwhile, for the training of this network, we have carefully designed a high-quality seismic training dataset. Synthetic clean records are constructed using the forward modeling method. The field seismic noise is superimposed on the dataset to guarantee the generalization of the training data. After processing the synthetic records and the field records, the results show that DBD-Net has a better performance in suppressing complex DAS background noise, coupled with an enhanced ability to accurately recover the effective signal, especially up-going signals with weak energy. Therefore, DBD-Net proves effective in suppressing strong DAS background noise and demonstrates notable application potential.

## Acknowledgments

None.

## Funding

This research was supported in part by the CNPC Science Research and Technology Development Project (2021DJ3505) and the Science and Technology Project of PetroChina Company Limited (2022KT1501).

## Conflict of interest

Haoliang Chen is employed by Northeast Electric Power Design Institute CO., LTD. of the China Power Engineering Consulting Group. The remaining authors declare no conflict of interest.

## Author contributions

*Conceptualization:* Wei Wang

*Formal analysis:* Wei Wang

*Investigation:* Wei Wang

*Methodology:* Wei Wang, Dekuan Chang

*Software:* Dong Li

*Validation:* Shujiang Wang

*Writing—original draft:* Haoliang Chen

*Writing—review & editing:* Xinyang Wang

## Availability of data

The data analyzed for this study are included in the article. Further inquiries can be directed to the corresponding author.

## References

1. Ashry I, Mao Y, Alias MS, *et al.* Normalized differential method for improving the signal-to-noise ratio of a distributed acoustic sensor. *Appl Opt.* 2019;58(18): 4933–4938.  
doi: 10.1364/AO.58.004933
2. Ashry I, Mao Y, Wang B, *et al.* A review of distributed fiber-optic sensing in the oil and GAS industry. *J Lightwave Technol.* 2022;40(5):1407–1431.  
doi: 10.1109/JLT.2021.3135653
3. Zhong T, Cheng M, Dong X, Li Y, Wu N. Seismic random noise suppression by using deep residual U-Net. *J Petrol Sci Eng.* 2022;209:109901.  
doi: 10.1016/j.petrol.2021.109901
4. Zhong T, Wang W, Lu S, Dong X, Yang B. RMCHN: A residual modular cascaded heterogeneous network for noise suppression in DAS-VSP records. *IEEE Geosci Remote Sens Lett.* 2023;20:1–5.  
doi: 10.1109/LGRS.2022.3229556
5. Cooper HW, Cook RE. Seismic data gathering. *Proc IEEE.* 1984;72(10):1266–1275.
6. Zhang Z, Alajami M, Alkhalifah T. Wave-equation dispersion



- spectrum inversion for near-surface characterization using fiber-optics acquisition. *Geophys J Int.* 2020;222(2):907-918.  
doi: 10.1093/gji/ggaa211
7. Spikes KT, Tisato N, Hess TE, Holt JW. Comparison of geophone and surface-deployed distributed acoustic sensing seismic data. *Geophysics.* 2019;84(2):A25-A29.  
doi: 10.1190/geo2018-0528.1
  8. Zhong T, Cheng M, Dong X, Wu N. Seismic random noise attenuation by applying multi-scale denoising convolutional neural network. *IEEE Trans Geosci Remote Sens.* 2022;60:590501.  
doi: 10.1109/TGRS.2021.3095922
  9. Dong X, Li Y. Denoising the optical fiber seismic data by using convolutional adversarial network based on loss balance. *IEEE Trans Geosci Remote Sens.* 2021;59(12):10544-10554.  
doi: 10.1109/TGRS.2020.3036065
  10. Zhong T, Cheng M, Lu S, Dong X, Li Y. RCEN: A deep-learning-based background noise suppression method for DAS-VSP records. *IEEE Geosci Remote Sens Lett.* 2022;19:3004905.  
doi: 10.1109/LGRS.2021.3127637
  11. Stockwell R, Manisinha L, Lowe R. Localization of the complex spectrum: The S transform. *IEEE Trans Signal Process.* 1996;44(4):998-1001.  
doi: 10.1109/78.492555
  12. Liu N, Gao J, Zhang B, Wang Q, Jiang X. Self-adaptive generalized S-transform and its application in seismic time-frequency analysis. *IEEE Trans Geosci Remote Sens.* 2019;57(10):7849-7859.  
doi: 10.1109/TGRS.2019.2916792
  13. Bekara M, van der Baan M. Random and coherent noise attenuation by empirical mode decomposition. *Geophysics.* 2009;74(5):V89-V98.
  14. Guo K, Labate D. Optimally sparse multidimensional representation using shearlets. *SIAM J Math Anal.* 2007;39(1):298-318.  
doi: 10.1137/060649781
  15. Houska R. The nonexistence of Shearlet scaling functions. *Appl Computat Harmon Anal.* 2012;32(1):28-44.  
doi: 10.1016/j.acha.2011.03.001
  16. Anvari R, Siahshar M, Gholtashi S, Kahoo A. Seismic random noise attenuation using synchrosqueezed wavelet transform and low-rank signal matrix approximation. *IEEE Trans Geosci Remote Sens.* 2017;55(11):6574-6581.  
doi: 10.1109/TGRS.2017.2730228
  17. Anvari R, Mohammadi M, Kahoo AR, Khan NA, Abdullah AI. Random noise attenuation of 2-D seismic data based on sparse low-rank estimation of the seismic signal. *Comput Geosci.* 2020;135:104376-104387.  
doi: 10.1016/j.cageo.2019.104376
  18. Binder G, Titov A, Liu Y, et al. Modeling the seismic response of individual hydraulic fracturing stages observed in a time-lapse distributed acoustic sensing vertical seismic profiling survey. *Geophysics.* 2020;85(4):T225-T235.  
doi: 10.1190/GEO2019-0819.1
  19. Wang Y, Liu X, Gao F, Rao Y. Robust vector median filtering with a structure-adaptive implementation. *Geophysics.* 2020;85(5):V407-V414.  
doi: 10.1190/GEO2020-0012.1
  20. Mendel JM. White-noise estimators for seismic data processing in oil exploration. *IEEE Trans Automat Control.* 2003;AC-22(5):694-706.  
doi: 10.1109/TAC.1977.1101597
  21. Han JJ, van der Baan M. Microseismic and seismic denoising via ensemble empirical mode decomposition and adaptive thresholding. *Geophysics.* 2015;80(6):69-80.  
doi: 10.1190/GEO2014-0423.1
  22. Liu N, Li F, Wang D, Gao J, Xu Z. Ground-roll separation and attenuation using curvelet-based multichannel variational mode decomposition. *IEEE Trans Geosci Remote Sens.* 2022;60:5901214.  
doi: 10.1109/TGRS.2021.3054749
  23. Yu S, Ma J. Complex variational mode decomposition for slope-preserving denoising. *IEEE Trans Geosci Remote Sens.* 2017;56(1):586-597.  
doi: 10.1109/TGRS.2017.2751642
  24. Bekara M, van der Baan M. Local singular value decomposition for signal enhancement of seismic data. *Geophysics.* 2007;72(2):V59-V65.
  25. Liu P, Li R, Yue YH, Liao SJ, Qian F. Robust prestack seismic facies analysis using shearlet transform-based deep learning. *J Geophys Eng.* 2022;19(3):521-533.  
doi: 10.1093/jge/gxac015
  26. Liu C, Wang D, Sun J, Wang T. Crossline-direction reconstruction of multi-component seismic data with shearlet sparsity constraint. *J Geophys Eng.* 2018;15(5):1929-1942.  
doi: 10.1088/1742-2140/aac097
  27. Liu Y, Fomel S, Liu C. Signal and noise separation in prestack seismic data using velocity-dependent seislet transform. *Geophysics.* 2015;80(6):WD117-WD128.  
doi: 10.1190/GEO2014-0234.1
  28. Neelamani R, Baumstein AI, Gillard DG, Hadidi MT, Soroka WL. Coherent and random noise attenuation using the curvelet transform. *Lead Edge.* 2008;27(2):240-248.

29. Li Y, Wang H, Dong X. The denoising of desert seismic data based on cycle-GAN with unpaired data training. *IEEE Geosci Remote Sens Lett.* 2021;18(11):2016-2020.  
doi: 10.1109/LGRS.2020.3011130
30. Dong X, Lin J, Lu S, Wang H, Li Y. Multiscale spatial attention network for seismic data denoising. *IEEE Trans Geosci Remote Sens.* 2022;60:21779964.  
doi: 10.1109/TGRS.2022.3178212
31. Dong X, Lin J, Lu S, Huang X, Wang H, Li Y. Seismic shot gather denoising by using a supervised deep learning method with weak dependence on real noise data: A solution to the lack of real noise data. *Surv Geophys.* 2022;43(5):1363-1394.  
doi: 10.1007/s10712-022-09702-7
32. Zhong T, Li F, Zhang R, Dong X, Lu S. Multi-scale residual pyramid network for seismic background noise attenuation. *IEEE Trans Geosci Remote Sens.* 2022;60:5922014.  
doi: 10.1109/TGRS.2022.3217887
33. Lin Y, Theiler J, Wohlberg B. Physics-guided data-driven seismic inversion: Recent progress and future opportunities in full-waveform inversion. *IEEE Signal Process Mag.* 2023;40(1):115-133.  
doi: 10.1109/MSP.2022.3217658
34. Chen G, Yang W, Wang H, Zhou H, Huang X. Elastic full waveform inversion based on full-band seismic data reconstructed by dual deconvolution. *IEEE Geosci Remote Sens Lett.* 2022;19:1-5.  
doi: 10.1109/LGRS.2022.3178915
35. Li J, Ye M, Stankovic L, Stankovic V, Pytharouli S. Domain knowledge informed multitask learning for landslide-induced seismic classification. *IEEE Geosci Remote Sens Lett.* 2023;20:1-5.  
doi: 10.1109/LGRS.2023.3279068
36. Noh K, Kim D, Byun J. Explainable deep learning for supervised seismic facies classification using intrinsic method. *IEEE Trans Geosci Remote Sens.* 2023;61:1-11.  
doi: 10.1109/TGRS.2023.3236500
37. Li X, Wu B, Zhu X, Yang H. Consecutively missing seismic data interpolation based on coordinate attention Unet. *IEEE Geosci Remote Sens Lett.* 2022;19:1-5.  
doi: 10.1109/LGRS.2021.3128511
38. Lu S. Migration using sea surface-related multiples: Challenges and opportunities. *Geophysics.* 2021;86(5):WC11-WC19.  
doi: 10.1190/GEO2020-0862.1
39. Lu S, Wu H, Dong X, *et al.* Building adjoint operators for least-squares migration using the acoustic wave equation. *Geophysics.* 2023;88(2):S71-S85.  
doi: 10.1190/GEO2022-0279.1
40. Wang H, Lin J, Dong X, Li Y, Yang B. Seismic velocity inversion transformer. *Geophysics.* 2023;88(4):R513-R533.  
doi: 10.1190/GEO2022-0283.1
41. Dong X, Cheng M, Wang H, Li G, Lin J, Lu S. A potential solution to insufficient target-domain noise data: Transfer learning and noise modeling. *IEEE Trans Geosci Remote Sens.* 2023;61:5915115.  
doi: 10.1109/TGRS.2023.3300697
42. Liu N, Wang J, Gao J, Chang S, Lou Y. Similarity-informed self-learning and its application on seismic image denoising. *IEEE Trans Geosci Remote Sens.* 2022;60:1-13.  
doi: 10.1109/TGRS.2022.3210217
43. Zhang K, Zuo W, Chen Y, Meng D, Zhang L. Beyond a Gaussian denoiser: Residual learning of deep CNN for image denoising. *IEEE Trans Image Process.* 2017;26(7):3142-3155.  
doi: 10.1109/TIP.2017.2662206
44. Olaf R, Philipp F, Thomas B. U-Net: Convolutional Networks for Biomedical Image Segmentation. In: *International Conference on Medical Image Computing and Computer-Assisted Intervention*. Cham: Springer International Publishing; 2015. p234-241.